Electronic Supplementary Material (ESI) for Dalton Transactions.

Asymmetric Oxidation of Bridging Vinyl- and Ethynyl Terthiophene Ligands in Trinuclear Ruthenium Complexes

Jing Zhang,[a] Chao-Fang Sun,[a] Ming-Xing Zhang,[a] František Hartl,*[,b] Jun Yin,[a] Guang-Ao Yu,[a] Li Rao,[a] Sheng Hua Liu*[,a]

[a]*Key Laboratory of Pesticide and Chemical Biology, Ministry of Education, College of Chemistry, Central China Normal University, Wuhan 430079, P.R. China*

[b]*Department of Chemistry, University of Reading, Whiteknights, Reading RG6 6AD, U.K.*

Electrochemistry

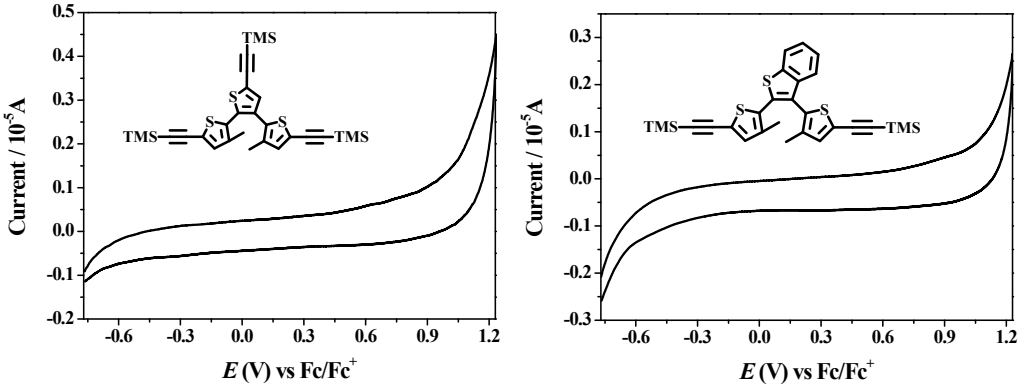

Figure S1. Cyclic voltammograms (CV) of the TMS-protected bridging ligand precursors in CH_2Cl_2/*n*-Bu_4NPF_6 at 10^{-1} V s^{-1}.

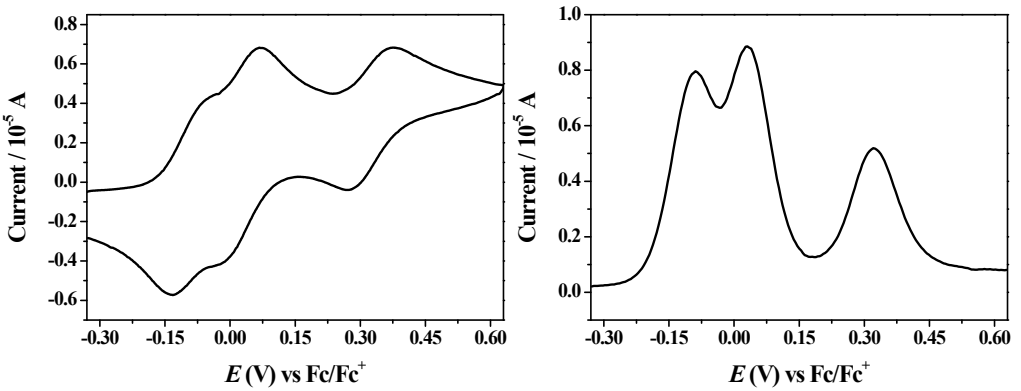

Figure S2. Left: cyclic voltammogram (CV) of complex **1d** in CH_2Cl_2/ *n*-$Bu_4N[B(C_6F_5)_4]$ at 10^{-1} V s^{-1}. Right: square-wave voltammogram (SWV) of complex **1d**, f = 10 Hz (t_p = 25 mV).

UV-Vis-NIR and IR Spectroelectrochemistry

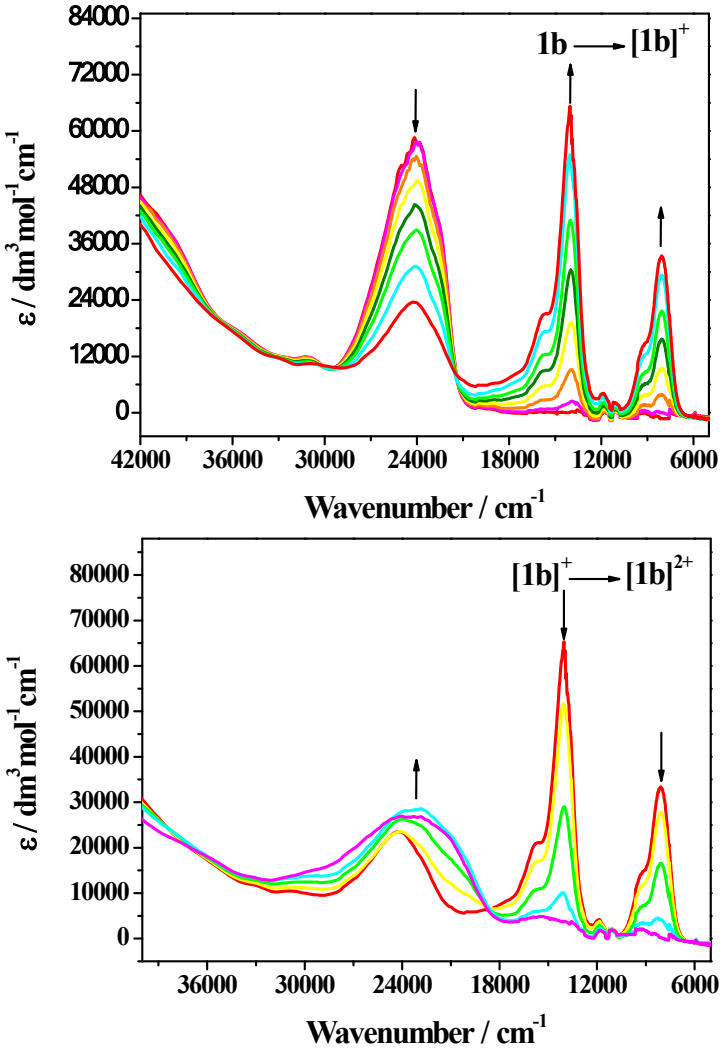

Figure S3. UV-vis-NIR spectral changes recorded during the successive oxidation of **1b** to [**1b**]$^{+}$ (top) and [**1b**]$^{2+}$ (bottom) in $CH_2Cl_2/10^{-1}$ M *n*-Bu_4NPF_6 at 298 K within an OTTLE cell.

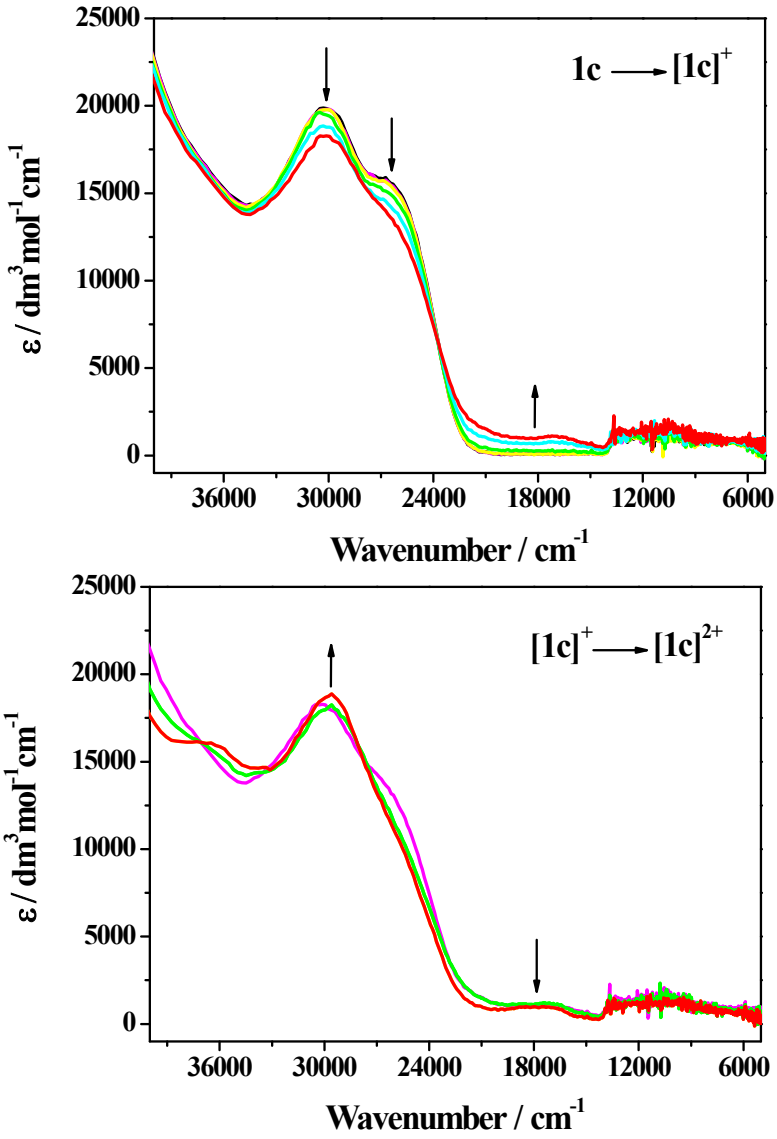

Figure S4. UV-vis-NIR spectral changes recorded during the successive oxidation of **1c** to [**1c**]$^{+}$ (top) and [**1c**]$^{2+}$ (bottom) in $CH_2Cl_2/10^{-1}$ M *n*-Bu_4NPF_6 at 298 K within an OTTLE cell.

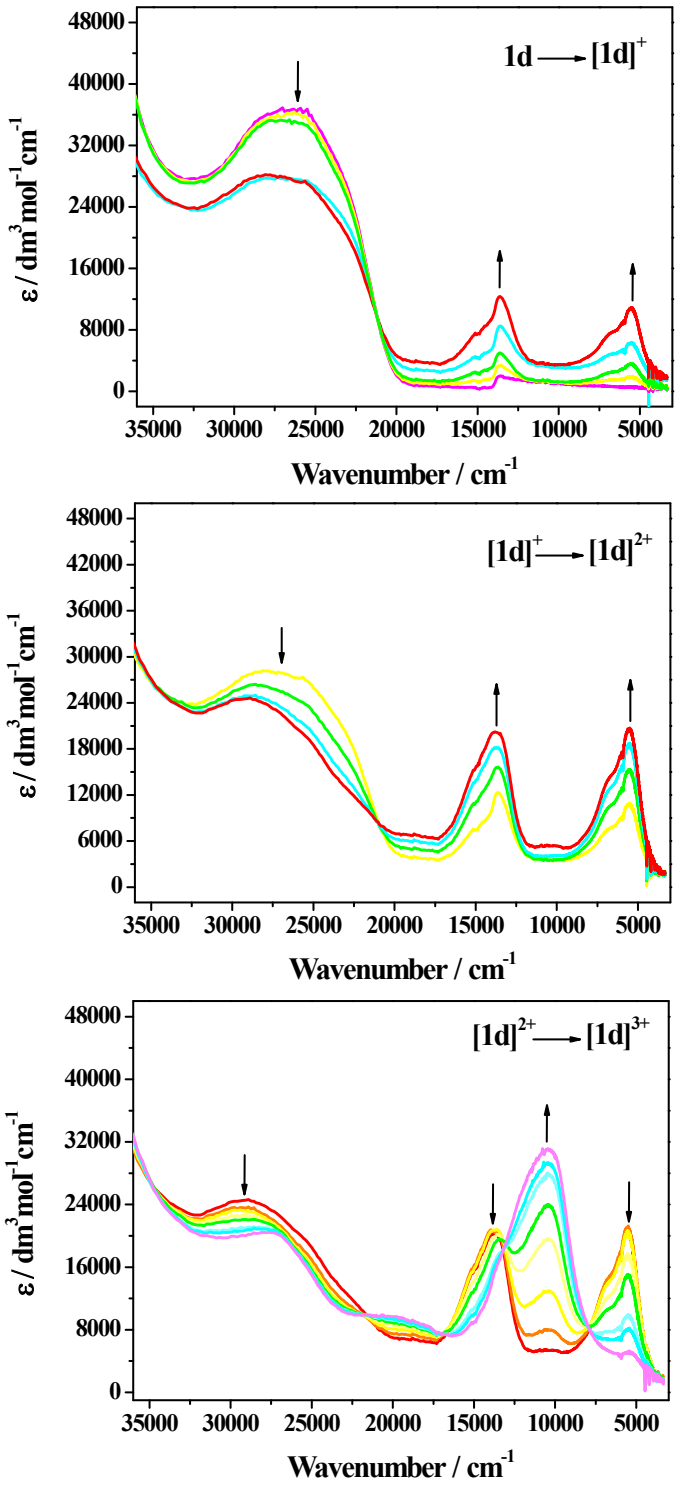

Figure S5. UV-vis-NIR spectral changes recorded during the stepwise oxidation of complex **1d** to [**1d**]$^{+}$ (top), [**1d**]$^{2+}$ (middle) and [**1d**]$^{3+}$ (bottom) in $CH_2Cl_2/10^{-1}$ M *n*-Bu_4NPF_6 at 298 K within an OTTLE cell.

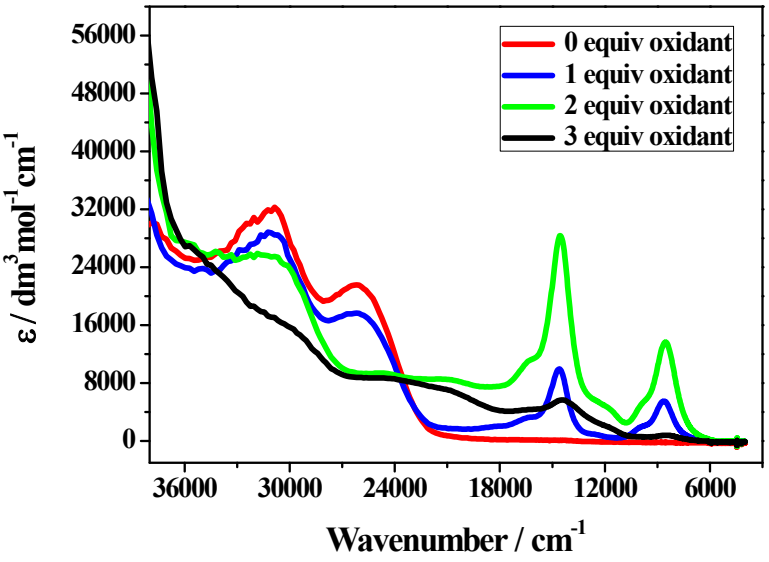

Figure S6. Electronic absorption spectra of **1a** (red), [**1a**]$^{+}$ (blue), [**1a**]$^{2+}$ (green) and [**1a**]$^{3+}$ (black) recorded in the course of stepwise oxidation of **1a** with thianthrenium hexafluorophosphate ($TAPF_6$) in CH_2Cl_2 at room temperature.

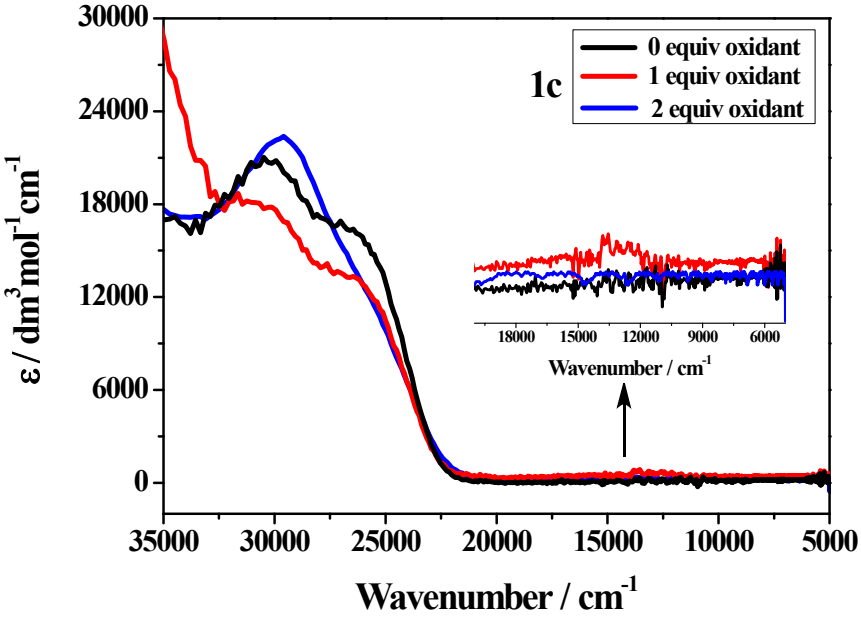

Figure S7. Electronic absorption spectra of **1c** (black), [**1c**]$^{+}$ (red) and [**1c**]$^{2+}$ (blue) recorded in the course of stepwise oxidation of **1c** with thianthrenium hexafluorophosphate ($TAPF_6$) in CH_2Cl_2 at room temperature.

DFT Calculations

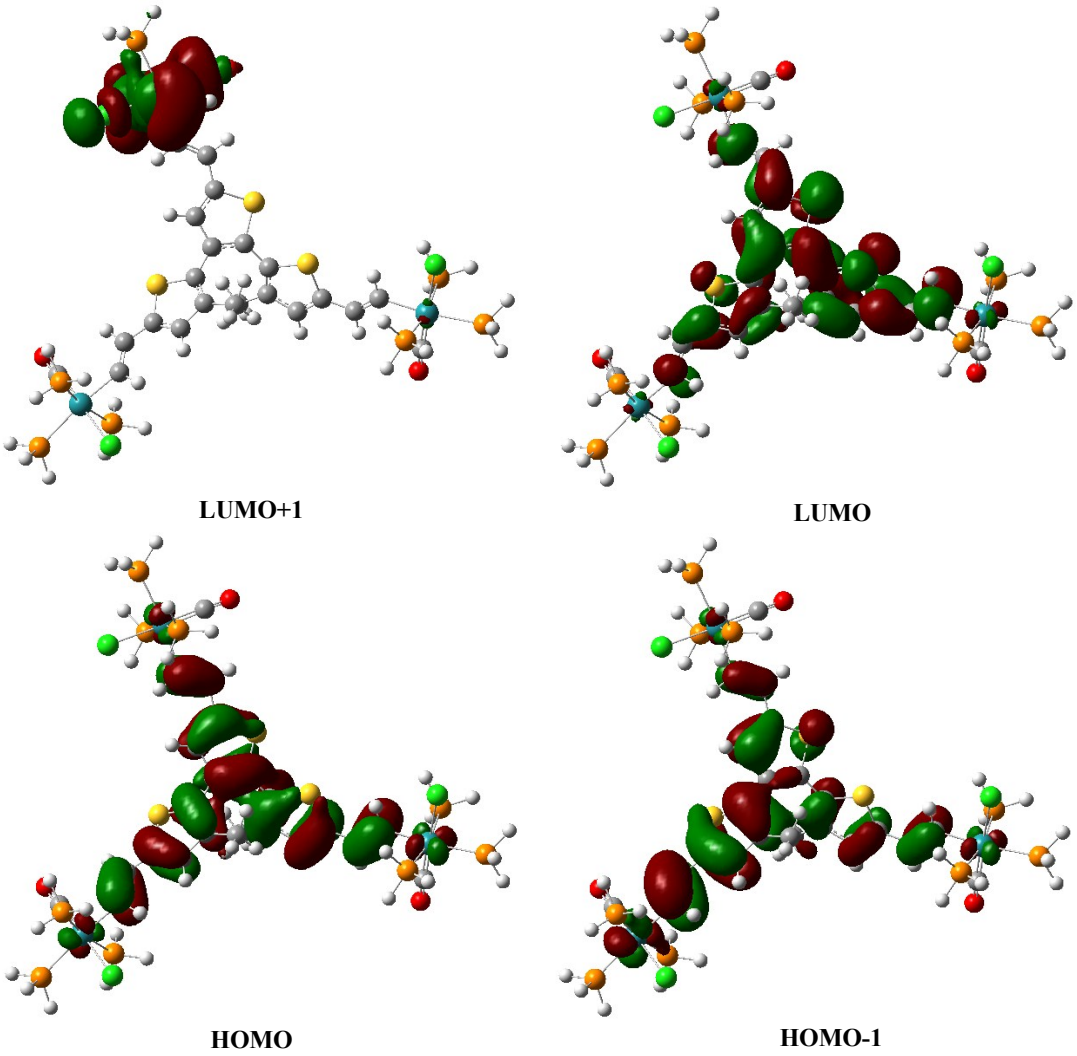

Figure S8. Selected frontier molecular orbitals of complex [**1a-H**] plotted with contour values ±0.04 $(e/bohr^3)^{1/2}$

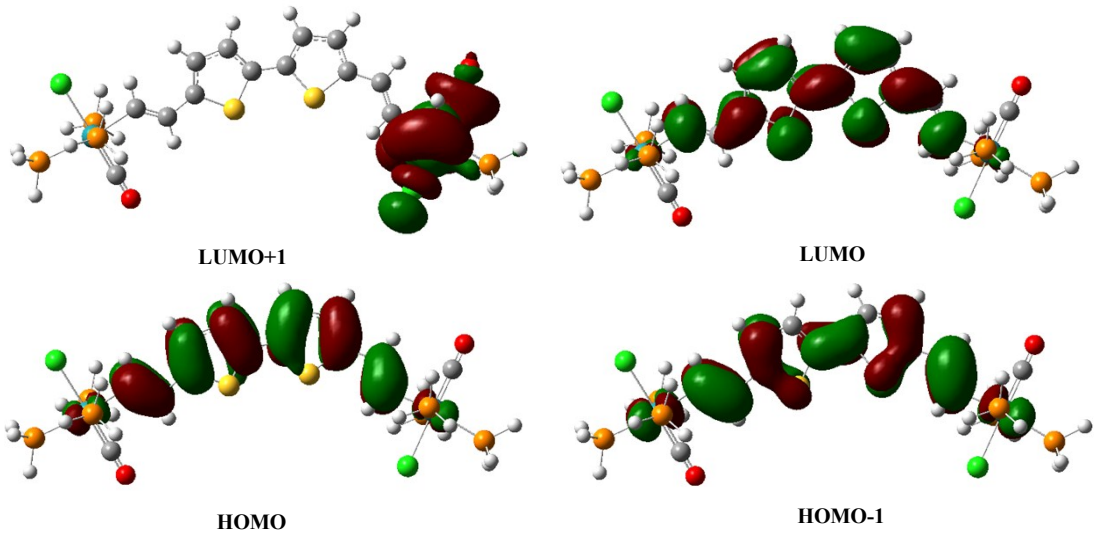

Figure S9. Selected frontier molecular orbitals of complex [**1b-H**] plotted with contour values ±0.04 $(e/bohr^3)^{1/2}$

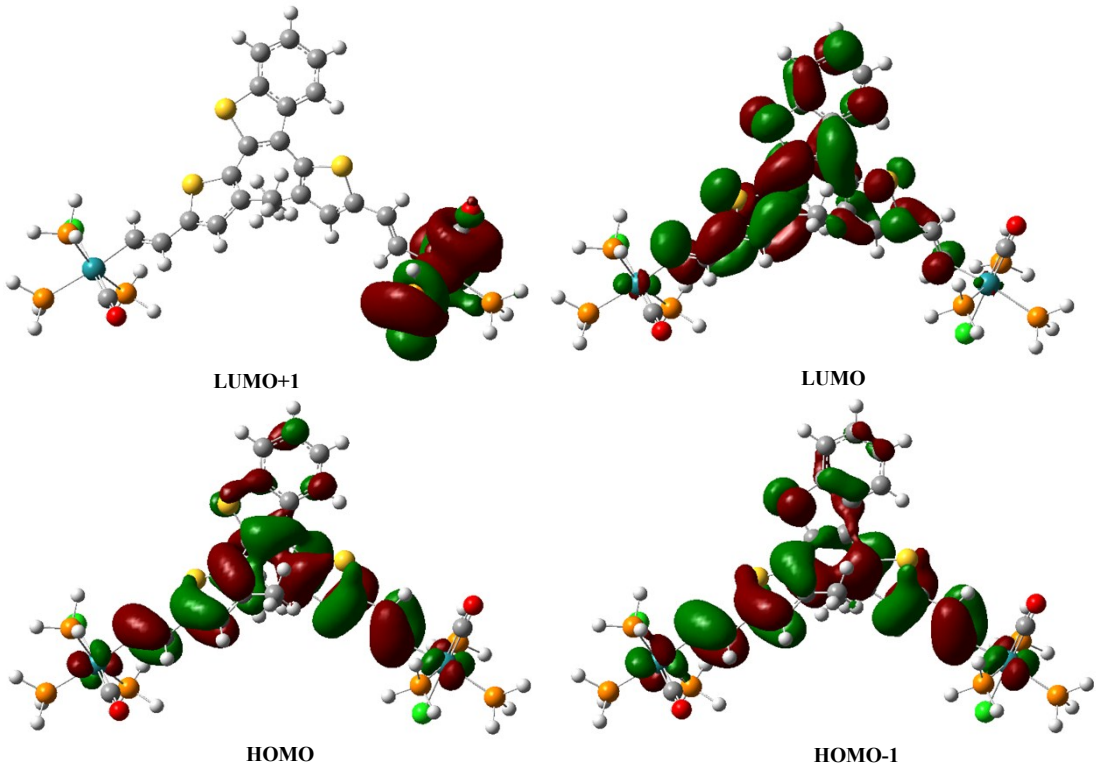

Figure S10. Selected frontier molecular orbitals of complex [**1c-H**] plotted with contour values ±0.04 $(e/bohr^3)^{1/2}$

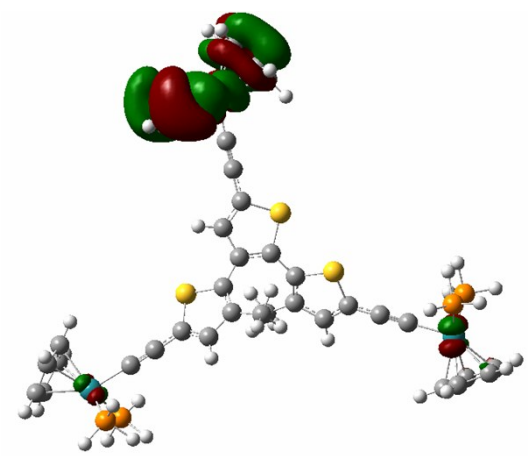

LUMO+1

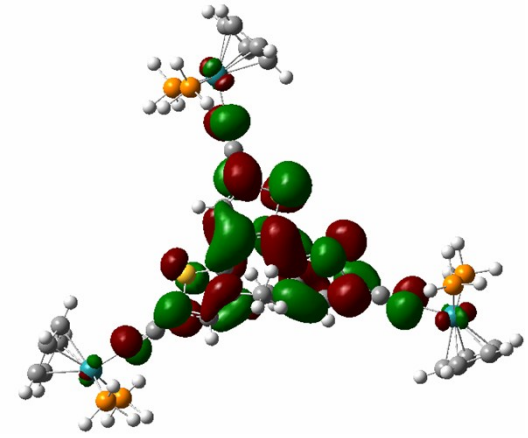

LUMO

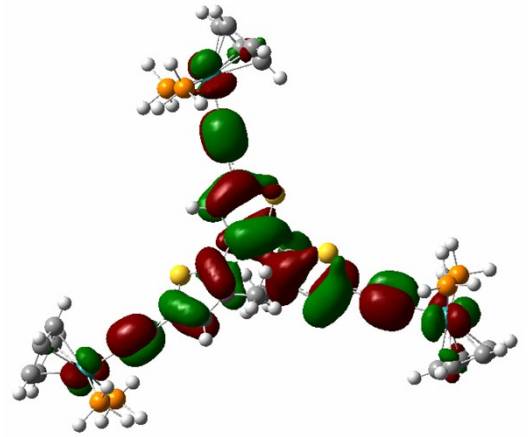

HOMO

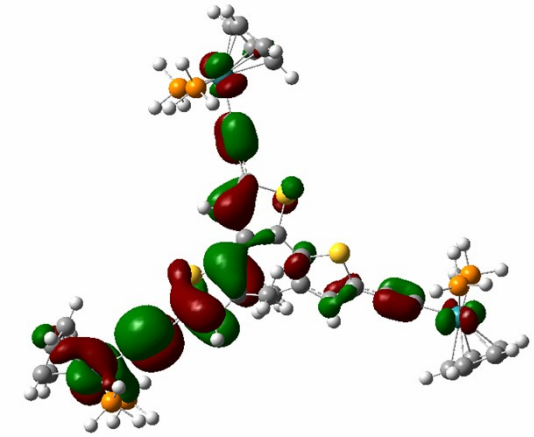

HOMO-1

Figure S11. Selected frontier molecular orbitals of complex [**1d-H**] plotted with contour values ±0.04 $(e/bohr^3)^{1/2}$

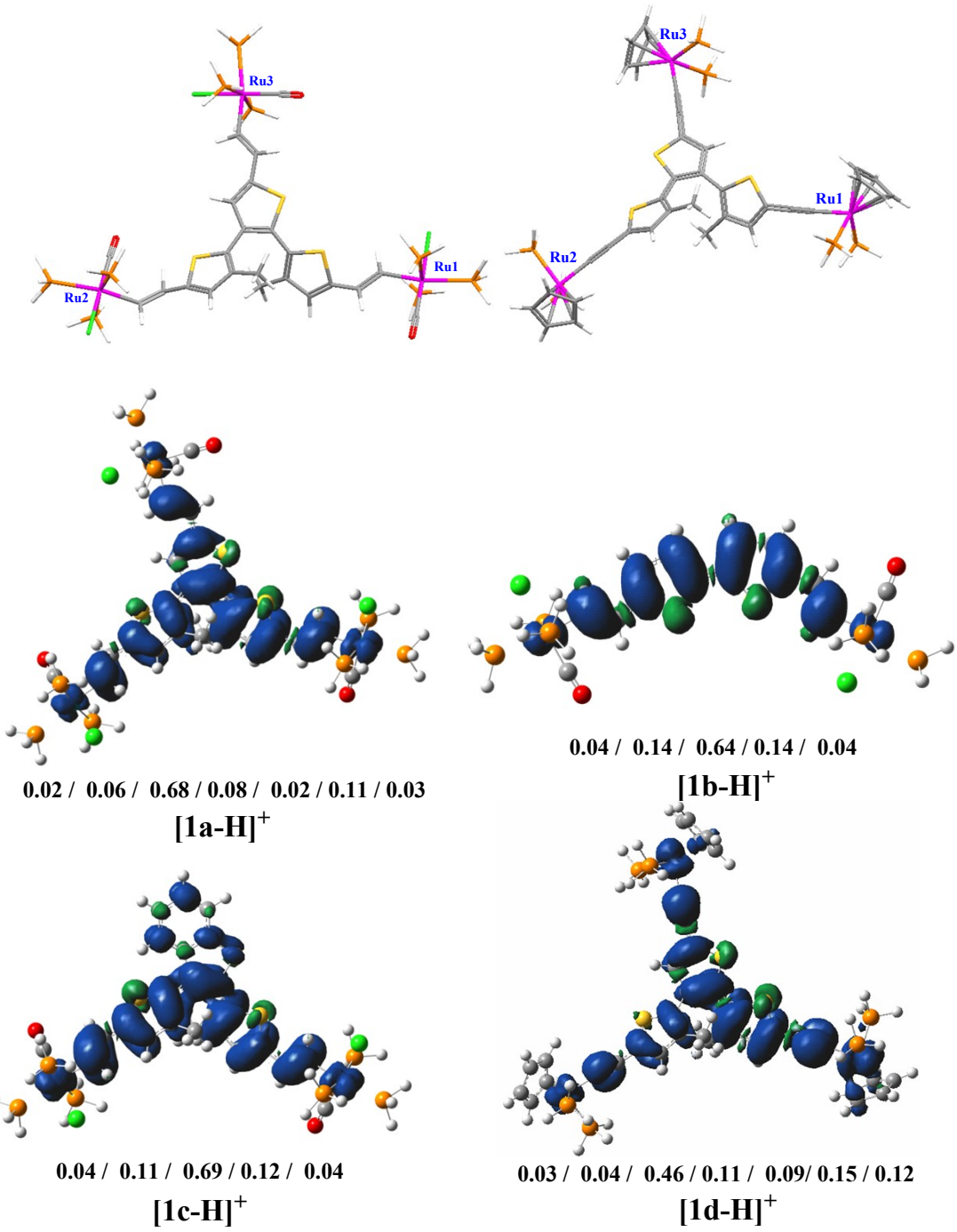

Figure S12. Spin-density distribution in [**1a-H**]$^+$ (Ru2/CH=CH/oligothiophene/CH=CH/Ru3/CH=CH/Ru1), [**1b-H**]$^+$ and [**1c-H**]$^+$ (Ru/CH=CH/oligothiophene/CH=CH/Ru), and [**1d-H**]$^+$ (Ru2/CH≡CH/oligothiophene/CH≡CH/Ru3/CH≡CH/Ru1) with the corresponding compositions. Contour values: ±0.04 $(e/bohr^3)^{1/2}$. B3LYP/6-31G* (Ru: Lanl2DZ) /CPCM /CH_2Cl_2.

Table S1. Energy and composition of frontier molecular orbitals of the model complex [**1a-H**] and [**1a-H**]$^{+}$. B3LYP / 6-31G* (Ru: Lanl2DZ) / CPCM / CH_2Cl_2.

[1a-H]

MO		eV	(CO)1	Cl1	$(PH_3)_2$1	Ru1	(C=C)1	$C_{14}H_9S_3$	(C=C)2	Ru2	$(PH_3)_2$2	Cl2	(CO)2	(CO)3	Cl3	$(PH_3)_2$3	Ru3	(C=C)3
245	L+1	-1.10	0	0	0	0	0	0	0	0	0	0	0	8	8	29	55	0
244	LUMO	-1.35	0	0	0	2	9	74	4	1	0	0	0	0	0	0	2	8
243	HOMO	-4.74	0	0	0	3	11	66	7	2	0	0	0	0	0	0	2	9
242	H-1	-5.19	0	0	0	2	5	60	22	6	0	0	0	0	0	0	1	4

[1a-H]$^{+}$

MO		eV	(CO)1	Cl1	$(PH_3)_2$1	Ru1	(C=C)1	$C_{14}H_9S_3$	(C=C)2	Ru2	$(PH_3)_2$2	Cl2	(CO)2	(CO)3	Cl3	$(PH_3)_2$3	Ru3	(C=C)3
243	β-LUSO	-4.32	0	0	0	3	11	69	5	1	0	0	0	0	0	0	2	9
242	β-HOSO	-5.56	0	0	0	1	3	54	26	8	0	0	0	0	0	0	2	6
241	β-HOSO-1	-6.09	0	0	0	9	19	41	0	0	0	0	0	0	0	0	10	21
233	β-HOSO-9	-7.13	0	2	0	4	2	74	2	8	0	0	0	0	0	0	5	3

Table S2. Energy and composition of frontier molecular orbitals of the model complexes [**1b-H**], [**1b-H**]$^{+}$, [**1b-H**]$^{2+}$ and [**1c-H**]. B3LYP / 6-31G* (Ru: Lanl2DZ) / CPCM / CH_2Cl_2.

	MO		eV	(CO)1	Cl1	$(PH_3)_2$1	Ru1	(C=C)1	oligothiophene	(C=C)2	Ru2	$(PH_3)_2$2	Cl2	(CO)2
[**1b-H**]	159	L+1	-1.10	8	8	29	55	0	0	0	0	0	0	0
	158	LUMO	-1.48	0	0	0	2	10	74	12	2	0	0	0
	157	HOMO	-4.69	0	0	0	3	14	66	14	3	0	0	0
	156	H-1	-5.74	0	0	0	9	22	36	23	10	0	0	0
[**1b-H**]$^{+}$	158	α-LUSO	-2.79	0	0	0	3	11	75	10	2	0	0	0
	157	α-HOSO	-5.59	0	0	0	6	15	56	16	7	0	0	0
	157	β-LUSO	-4.28	0	0	0	4	14	64	14	4	0	0	0
	156	β-HOSO	-6.23	0	0	0	11	19	38	21	11	0	0	0
[**1b-H**]$^{2+}$	158	L+1	-3.50	0	0	0	3	13	68	13	3	0	0	0
	157	LUMO	-5.12	0	0	0	5	15	58	16	6	0	0	0
	156	HOMO	-7.00	0	0	0	13	17	39	18	13	0	0	0
	155	H-1	-7.45	5	61	3	29	2	0	0	0	0	0	0
[**1c-H**]	201	L+1	-1.11	0	0	0	0	0	0	0	55	29	8	8
	200	LUMO	-1.43	0	0	0	2	10	84	3	1	0	0	0
	199	HOMO	-4.95	0	0	0	3	11	69	14	3	0	0	0
	198	H-1	-5.33	0	0	0	5	17	58	15	5	0	0	0

Table S3. Energy and composition of frontier molecular orbitals of the model complex [**1d-H**] and [**1d-H**]$^{+}$. B3LYP / 6-31G* (Ru: Lanl2DZ) / CPCM / CH_2Cl_2.

[**1d-H**]															
MO		eV	Cp 1	$(PH_3)_2$ 1	Ru 1	(C≡C) 1	$C_{14}H_9S_3$	Cp 2	$(PH_3)_2$ 2	Ru 2	(C≡C) 2	Cp 3	$(PH_3)_2$ 3	Ru 3	(C≡C) 3
221	L+1	-0.82	0	0	1	0	0	0	0	2	0	27	30	40	0
220	LUMO	-1.17	0	0	2	5	81	0	0	1	3	0	1	2	5
219	HOMO	-4.37	2	1	7	12	49	1	0	4	6	1	1	6	10
218	H-1	-4.74	0	0	3	3	38	4	2	18	23	0	0	4	5
[**1d-H**]$^{+}$															
MO		eV	Cp 1	$(PH_3)_2$ 1	Ru 1	(C≡C) 1	$C_{14}H_9S_3$	Cp 2	$(PH_3)_2$ 2	Ru 2	(C≡C) 2	Cp 3	$(PH_3)_2$ 3	Ru 3	(C≡C) 3
219	β-LUSO	-3.98	1	1	8	13	60	0	0	2	4	1	1	5	4
218	β-HOSO	-4.96	0	0	1	1	36	4	2	22	24	1	0	4	5
217	β-HOSO-1	-5.29	3	2	16	13	28	0	0	0	0	4	2	18	14
209	β-HOSO-9	-6.52	2	1	10	2	52	4	1	13	3	2	1	7	2

Table S4. Comparison of calculated IR ν(C≡O) and ν(C≡C) wavenumbers (cm^{-1}) (scaled by 0.95 and 0.9614 for BLYP35 and B3LYP, respectively) using different methods for [**1a-H**]$^{n+}$- [**1d-H**]$^{n+}$ (n = 0, 1, 2).

Vibration	Complex	BLYP35	B3LYP	Experiment
ν(C≡O)	**1a-H**	2251	1954	1922
	[**1a-H**]$^{+}$	2254sh, 2261	1965	1922
	[**1a-H**]$^{2+}$	2263m, 2269s, 2277m [a]	1972s, 1978m [a] 1999s, 2011m, sh [b]	1922
	1b-H	2251	1952	1923
	[**1b-H**]$^{+}$	2266	1965	1927
	[**1b-H**]$^{2+}$	2281	1985	1935
	1c-H	2251	1953	1923
	[**1c-H**]$^{+}$	2263	1965	1923
	[**1c-H**]$^{2+}$	2274	1978	1924
ν(C≡C)	**1d-H**	2318w	2071w	2051m
	[**1d-H**]$^{+}$	2255s, 2270m, 2298w	1980s, 2001m, 2046w	1935s, 1992w, 2049m-w
	[**1d-H**]$^{2+}$	2225s, 2239m, 2271w [a]	1956s, 1961s, 2014w [a] 1977s, 1997s, 2020w [b]	1935s, 1992w, 2046w

[a] Singlet. [b] Triplet.

Table S5. Major electronic excitations in [**1a-H**]$^+$-[**1d-H**]$^+$ determined by TD-DFT methods.[a]

Complex	Excited state	λ/nm [cm^{-1}]	Osc. str (f)	Major contributions	Assignment
[**1a-H**]$^+$	D_1	1170 [8547]	0.1888	β-HOSO→β-LUSO (98%)	bridge π–π* / MLCT
	D_2	863 [11587]	0.4766	β-HOSO-1→β-LUSO (96%)	bridge π–π* / MLCT
	D_3	574 [17421]	0.6029	α-HOSO→α-LUSO (75%)	bridge π–π*
[**1b-H**]$^+$	D_1	790 [12658]	0.3813	β-HOSO→β-LUSO (91%)	bridge π–π*/MLCT
				α-HOSO→α-LUSO (39%)	MLCT/ ML→LCT
	D_4	578 [17301]	1.4791	α-HOSO→α-LUSO (85%)	MLCT/ ML→LCT
	D_{10}	380 [26315]	0.0383	β-HOSO-5→β-LUSO (72%)	Cl →LCT
[**1c-H**]$^+$	D_1	1479 [6761]	0.3353	β-HOSO→β-LUSO (98%)	MLCT/ ML→LCT
	D_2	696 [14367]	0.1866	β-HOSO-1→β-LUSO (97%)	Cl →LCT
				α-HOSO→α-LUSO (64%)	MLCT
	D_3	562 [17793]	0.1557	β-HOSO→β-LUSO (23%)	MLCT/ ML→LCT
[**1d-H**]$^+$	D_1	1290 [7751]	0.2668	β-HOSO→β-LUSO (94%)	MLCT / bridge π–π*
	D_2	1213 [8244]	0.6604	β-HOSO-1→β-LUSO (94%)	MLCT/ bridge π–π*
	D_5	600 [16667]	0.0854	β-HOSO-2→β-LUSO (73%)	MLCT

[a] The computation method is BLYP35 / 6-31G* (Ru: Lanl2DZ) / CPCM / CH_2Cl_2. *D* = doublet.

Table S6. Major electronic excitations in [**1b-H**]$^+$ and [**1c-H**]$^+$ determined by TD-DFT methods.[a]

Complex	Excited state	λ/nm [cm^{-1}]	Osc. str (*f*)	Major contributions	Assignment
[**1b-H**]$^+$	D_1	923 [10834]	0.3381	β-HOSO→β-LUSO (91%)	bridge π–π* / MLCT
	D_2	606 [16501]	1.4867	α-HOSO→α-LUSO (87%)	bridge π–π* / MLCT
	D_9	461 [21691]	0.0112	β-HOSO→β-LUSO+1 (64%)	bridge π–π*
[**1c-H**]$^+$	D_2	844 [11848]	0.1283	β-HOSO-1→β-LUSO (99%)	ILCT/ bridge π–π*
	D_3	690 [14492]	0.1023	β-HOSO-3→β-LUSO (92%)	Cl →LCT/ bridge π–π*

[a] The computation method is B3LYP / 6-31G* (Ru: Lanl2DZ) / CPCM / CH_2Cl_2. *D* = doublet.

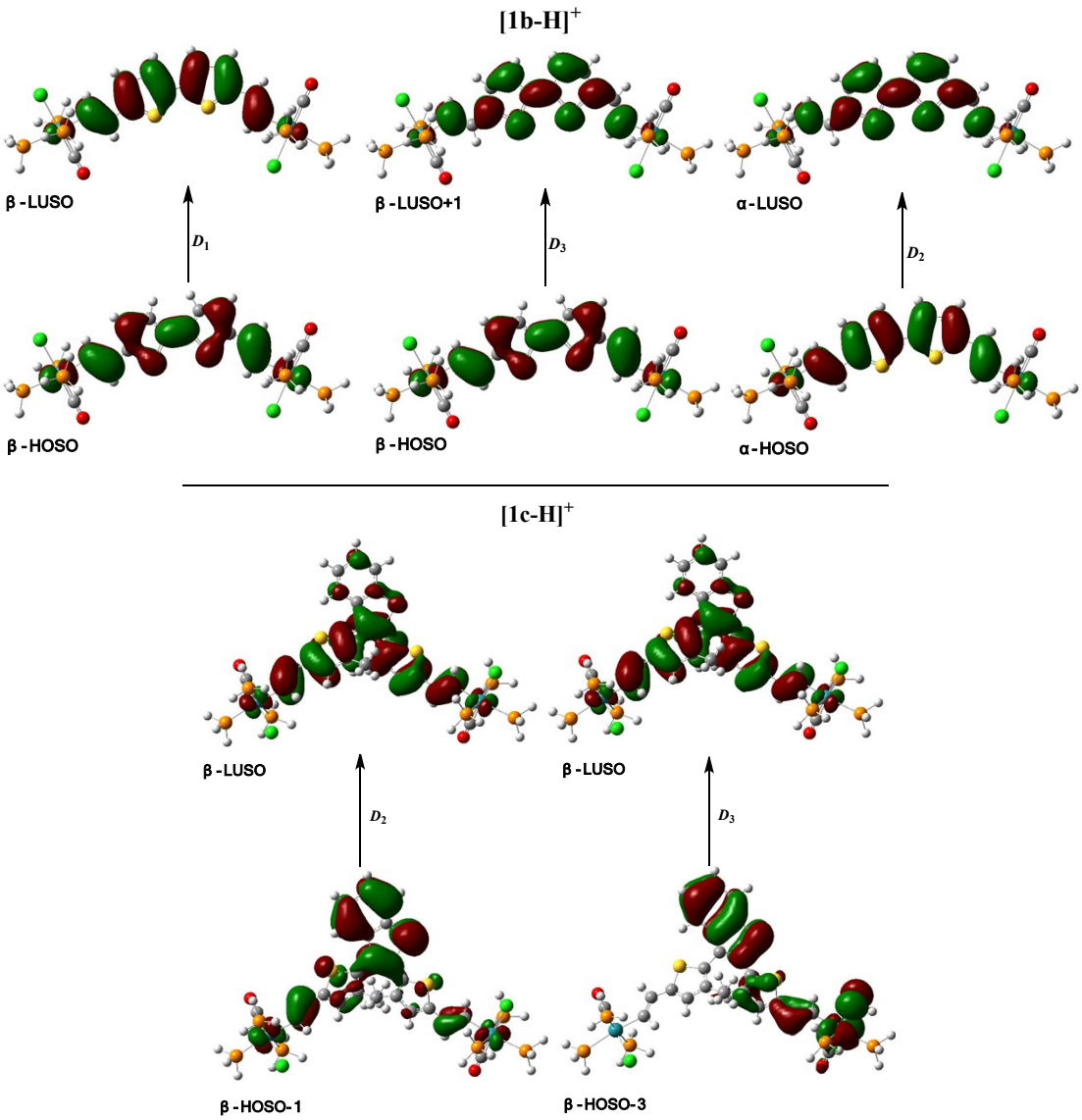

Figure S13. Spin orbitals involved in the major electronic excitations of [**1b-H**]$^+$ and [**1c-H**]$^+$ shown in Table S6 (*D* = doublet). B3LYP / 6-31G* (Ru: Lanl2DZ) / CPCM / CH_2Cl_2.

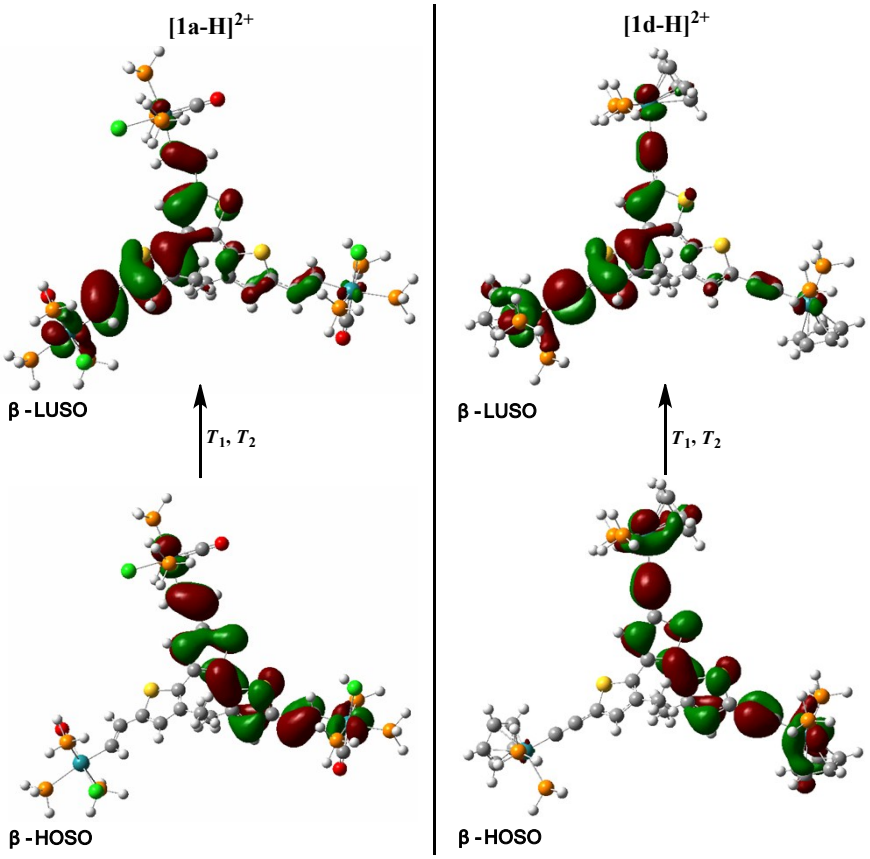

Figure S14. Spin orbitals involved in the electronic excitations of the main NIR absorptions for [**1a-H**]$^{2+}$ and [**1d-H**]$^{2+}$ shown in Table 4 (T = triplet). B3LYP / 6-31G* (Ru: Lanl2DZ) / CPCM / CH_2Cl_2.

NMR Spectra

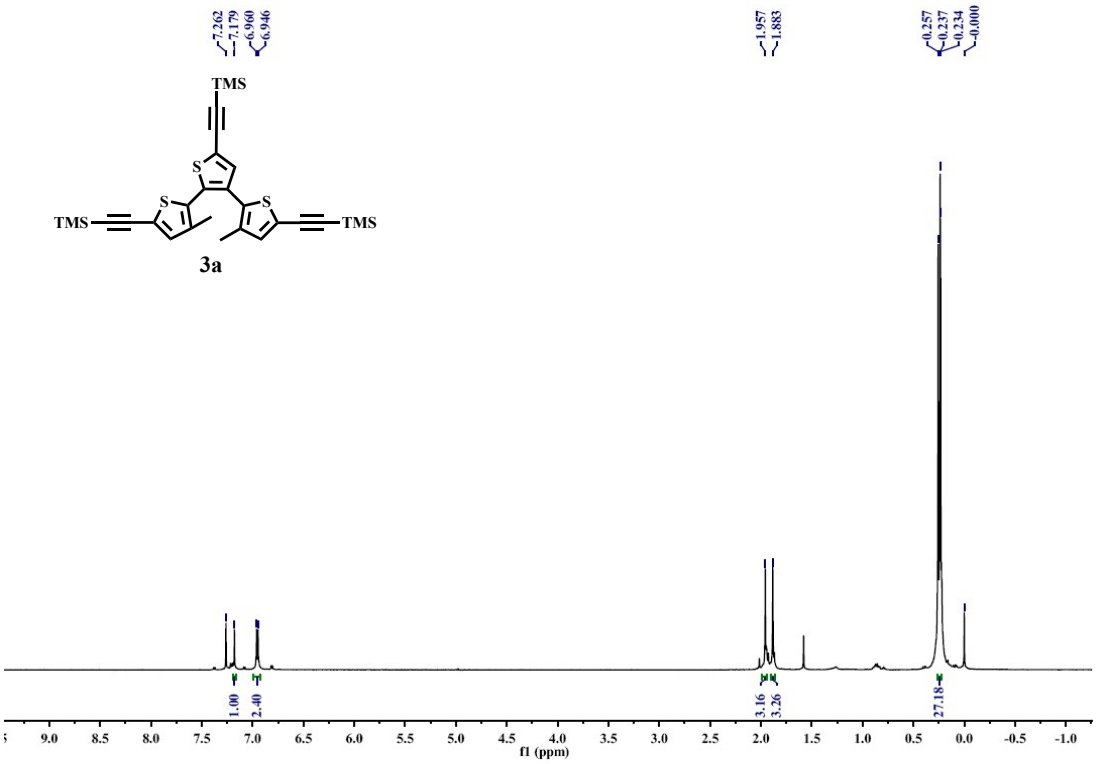

Figure S15. ^{1}H NMR spectrum (400 MHz, $CDCl_3$) of **3a**.

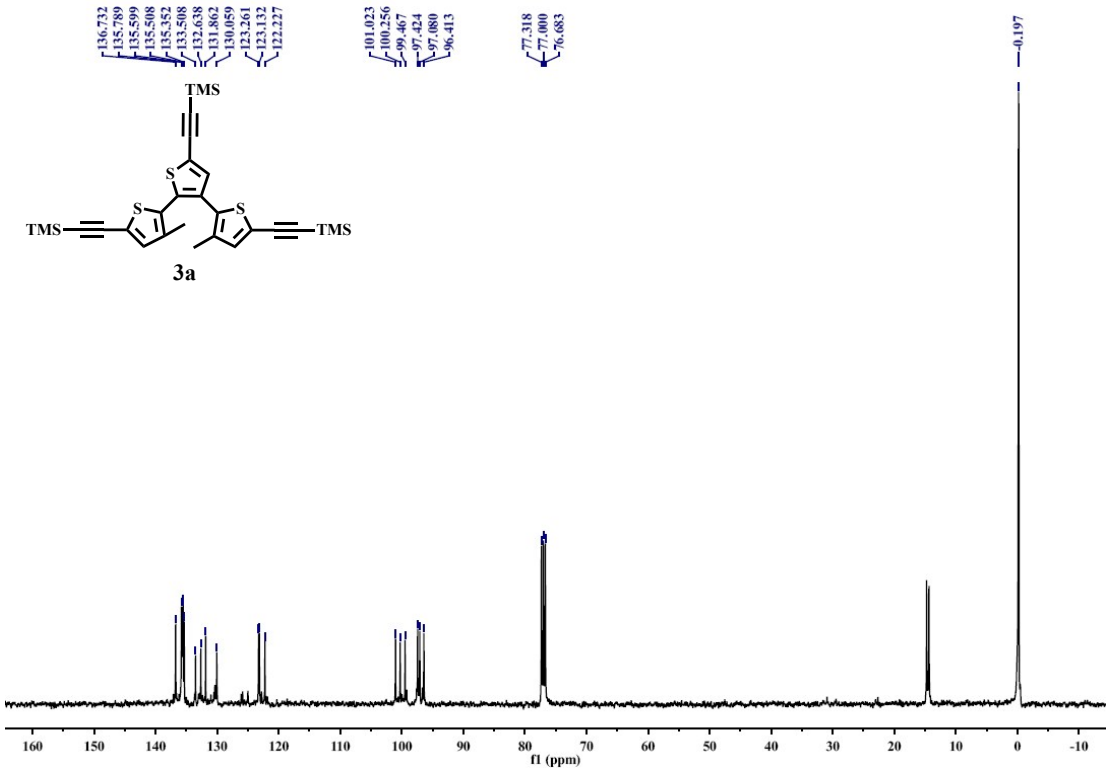

Figure S16. ^{13}C NMR spectrum (100 MHz, $CDCl_3$) of **3a**.

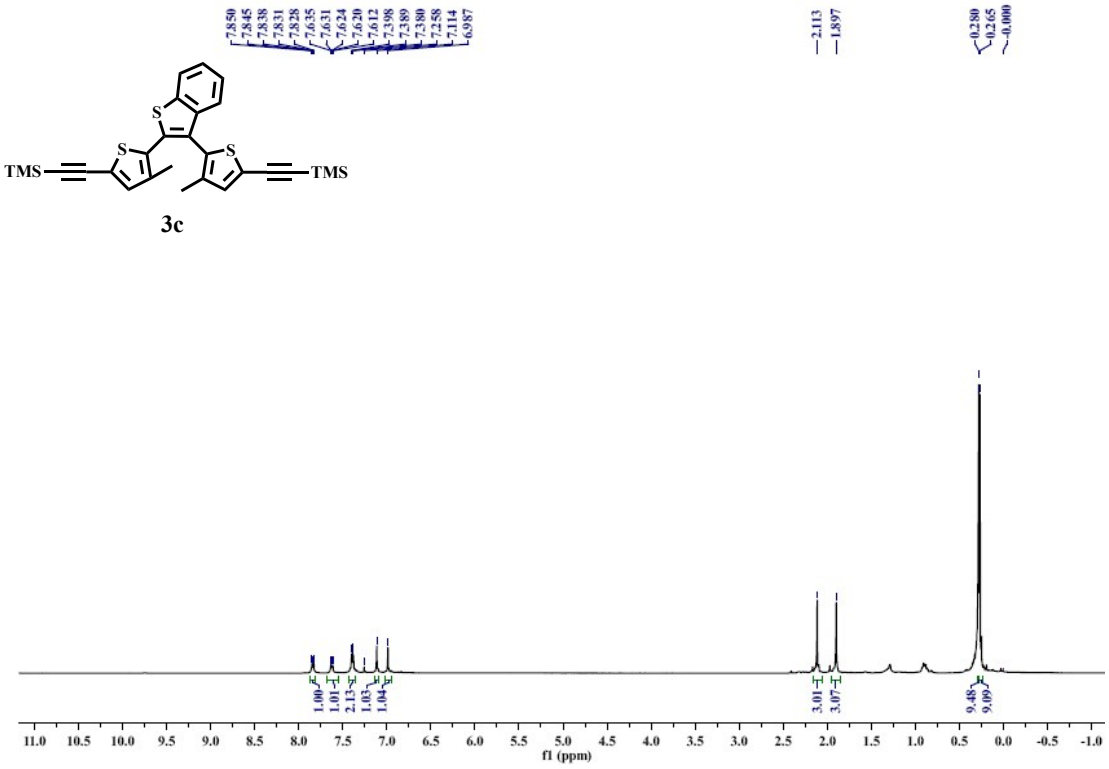

Figure S17. ^{1}H NMR spectrum (400 MHz, $CDCl_3$) of **3c**.

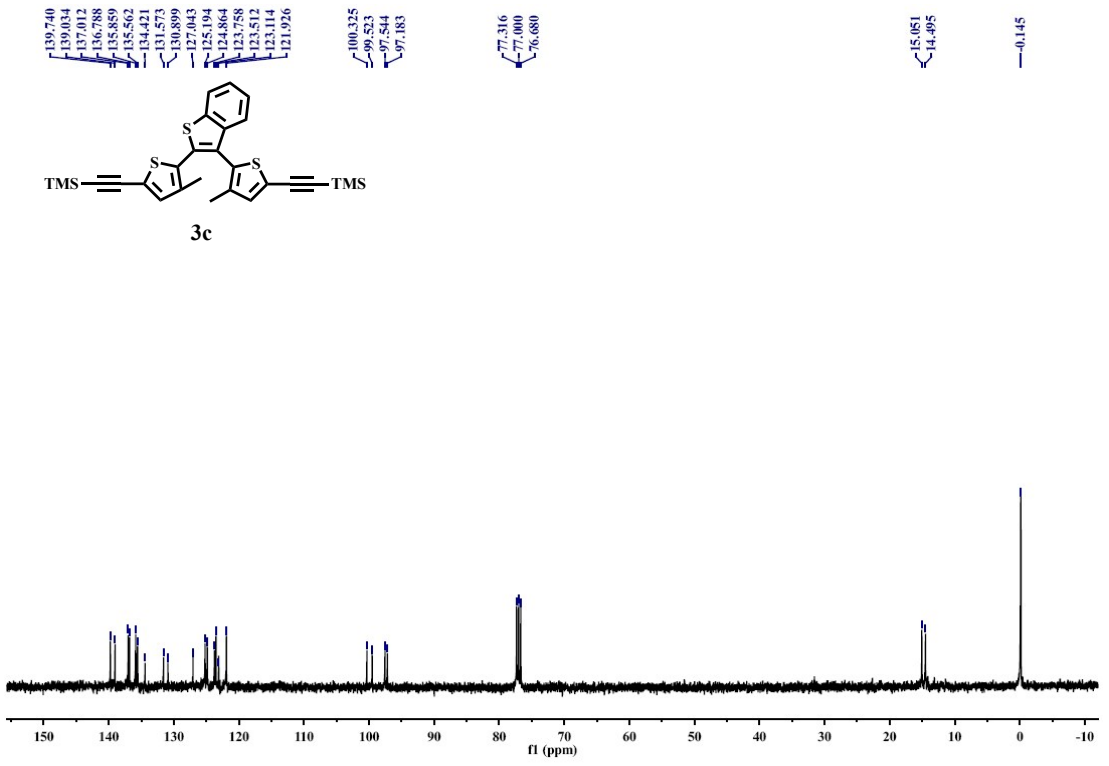

Figure S18. ^{13}C NMR spectrum (100 MHz, $CDCl_3$) of **3c**.

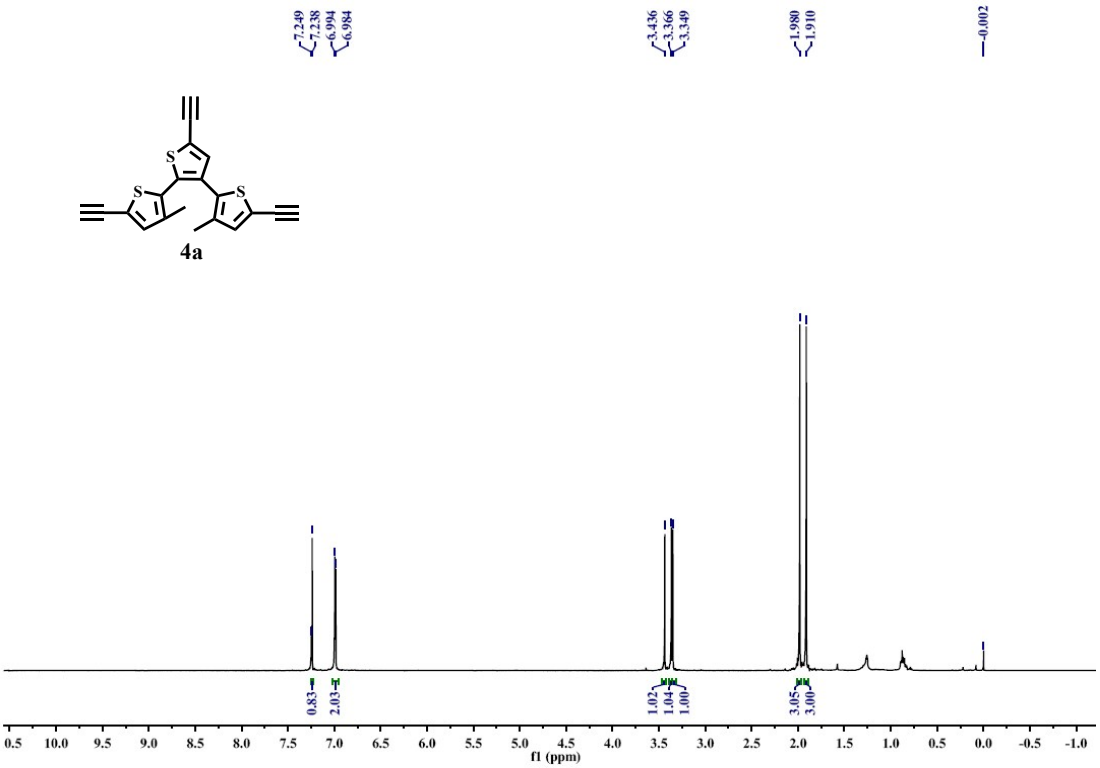

Figure S19. ^{1}H NMR spectrum (400 MHz, $CDCl_3$) of **4a**.

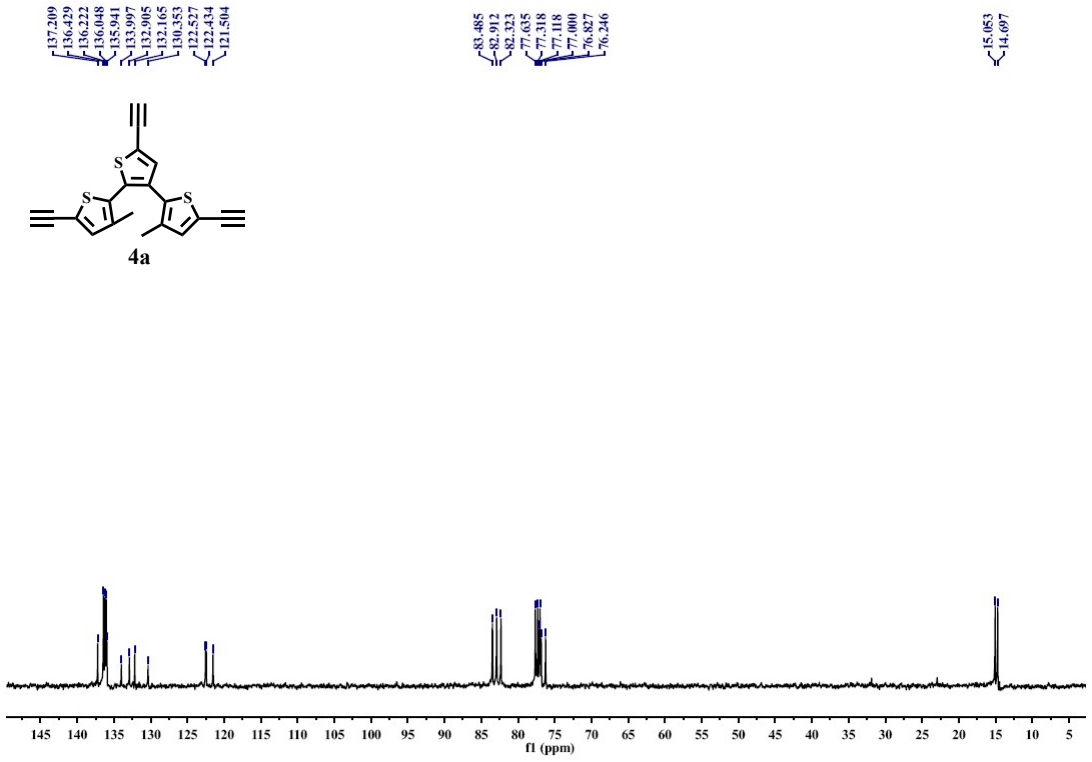

Figure S20. ^{13}C NMR spectrum (100 MHz, $CDCl_3$) of **4a**.

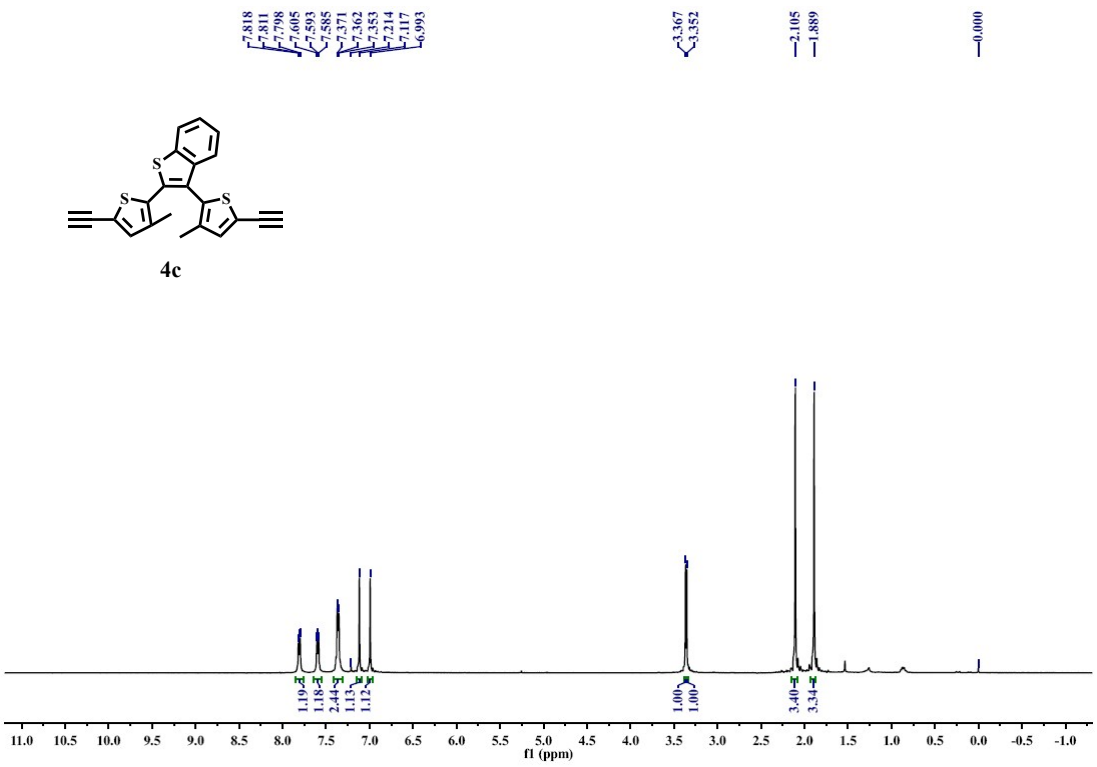

Figure S21. ^{1}H NMR spectrum (400 MHz, $CDCl_3$) of **4c**.

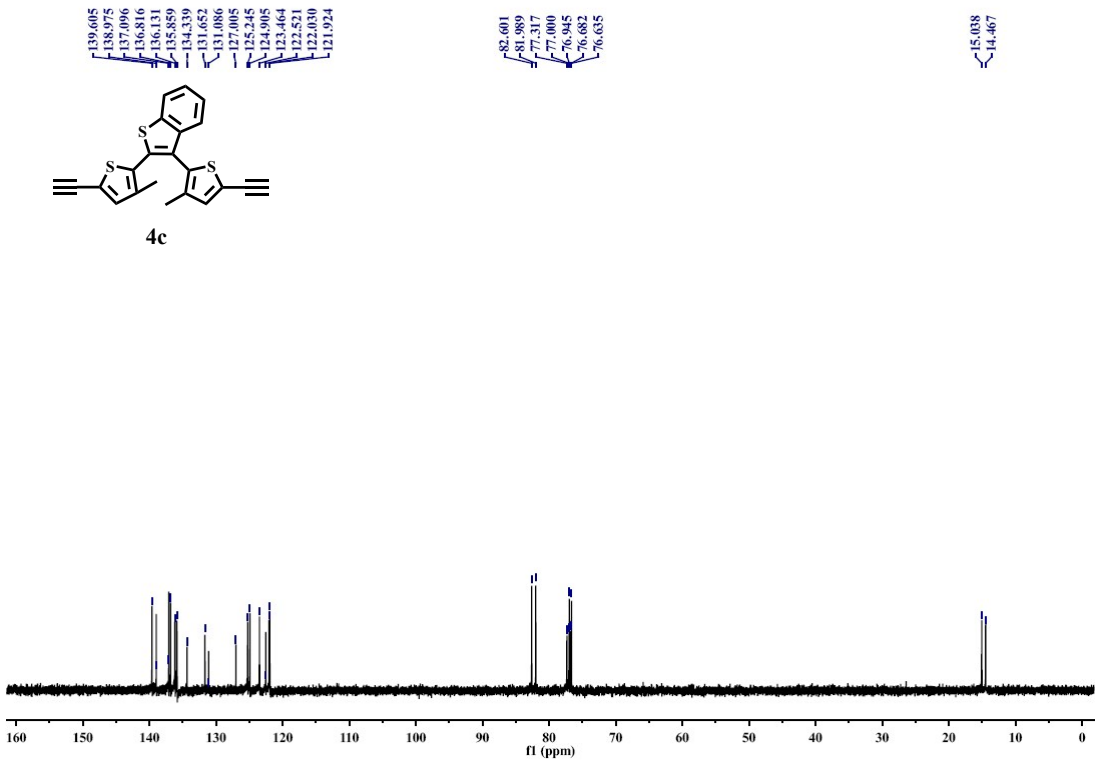

Figure S22. ^{13}C NMR spectrum (100 MHz, $CDCl_3$) of **4c**.

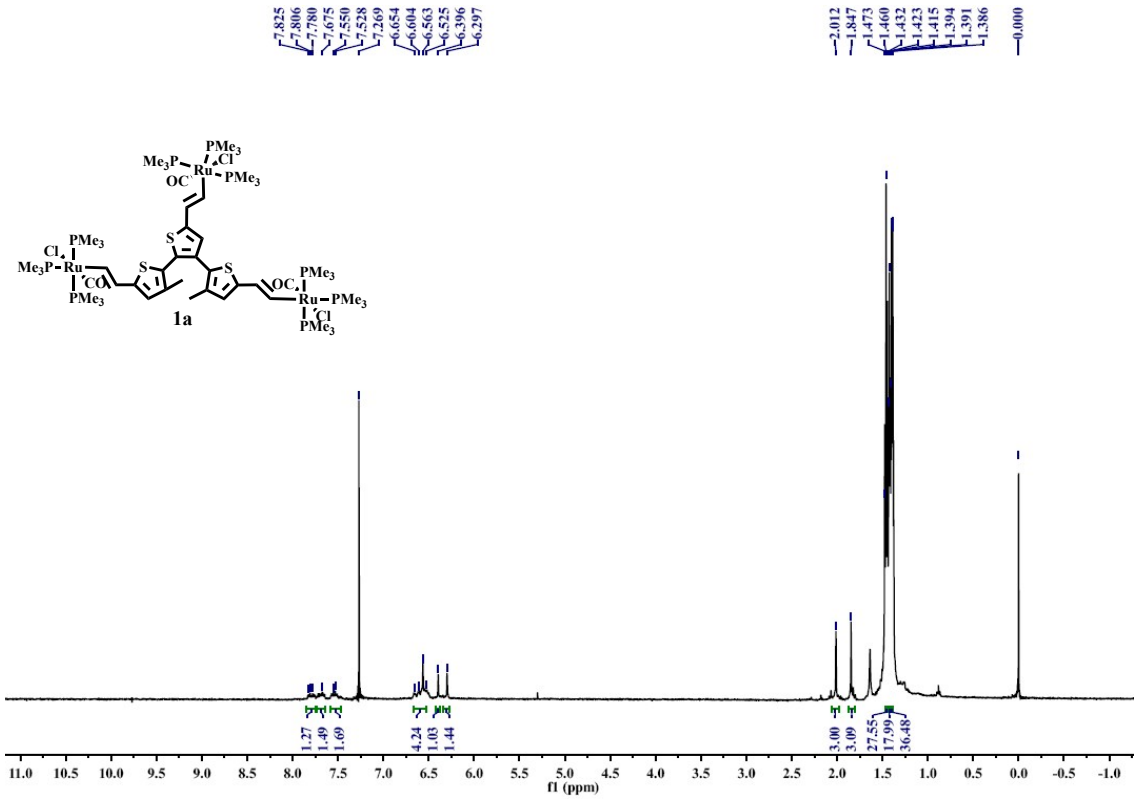

Figure S23. ^{1}H NMR spectrum (400 MHz, $CDCl_3$) of **1a**.

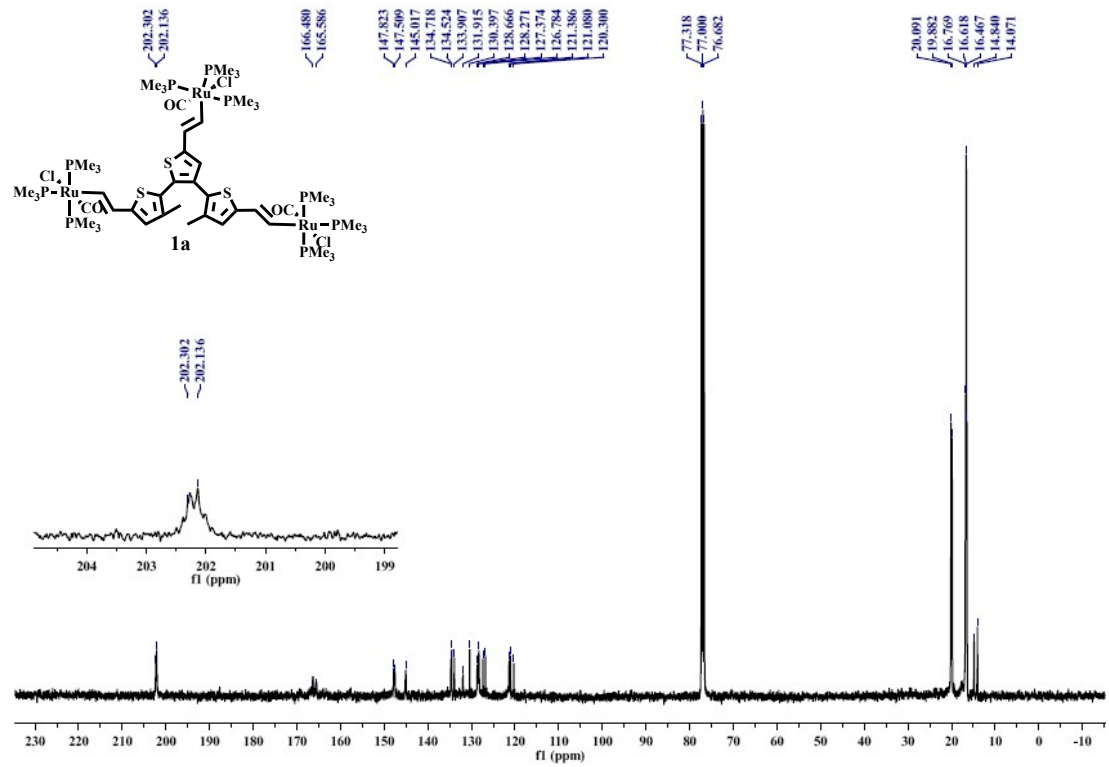

Figure S24. ^{13}C NMR spectrum (100 MHz, $CDCl_3$) of **1a**.

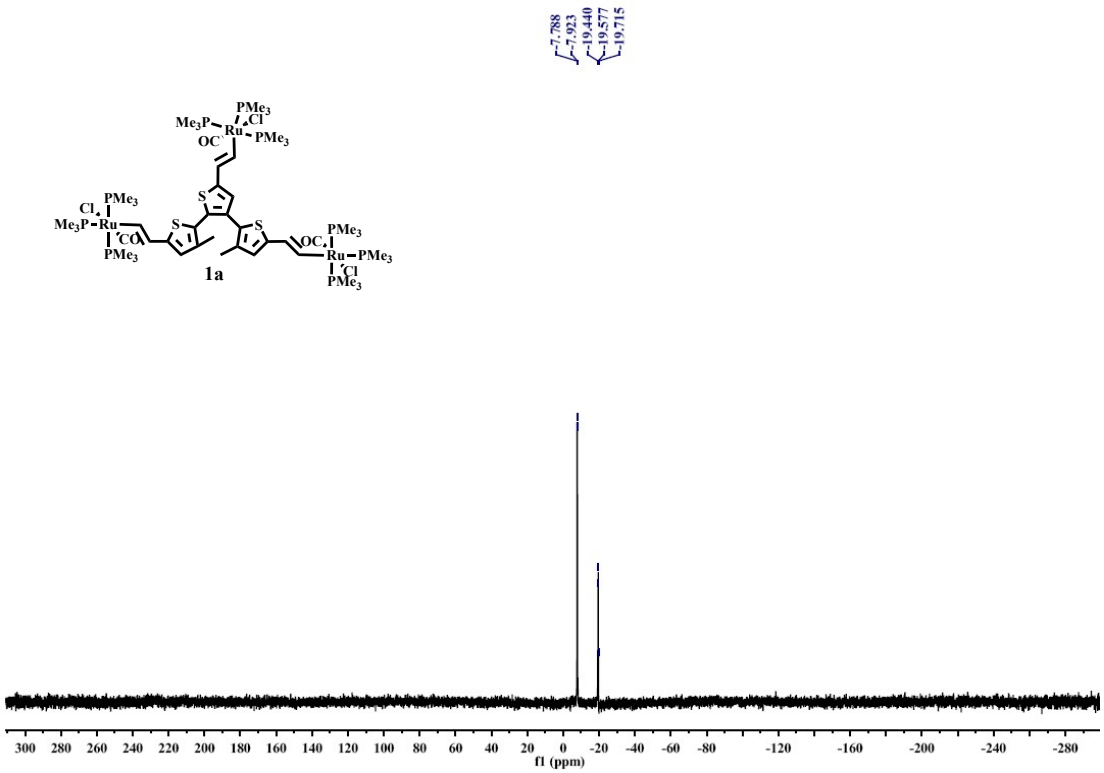

Figure S25. ^{31}P NMR spectrum (160 MHz, $CDCl_3$) of **1a**.

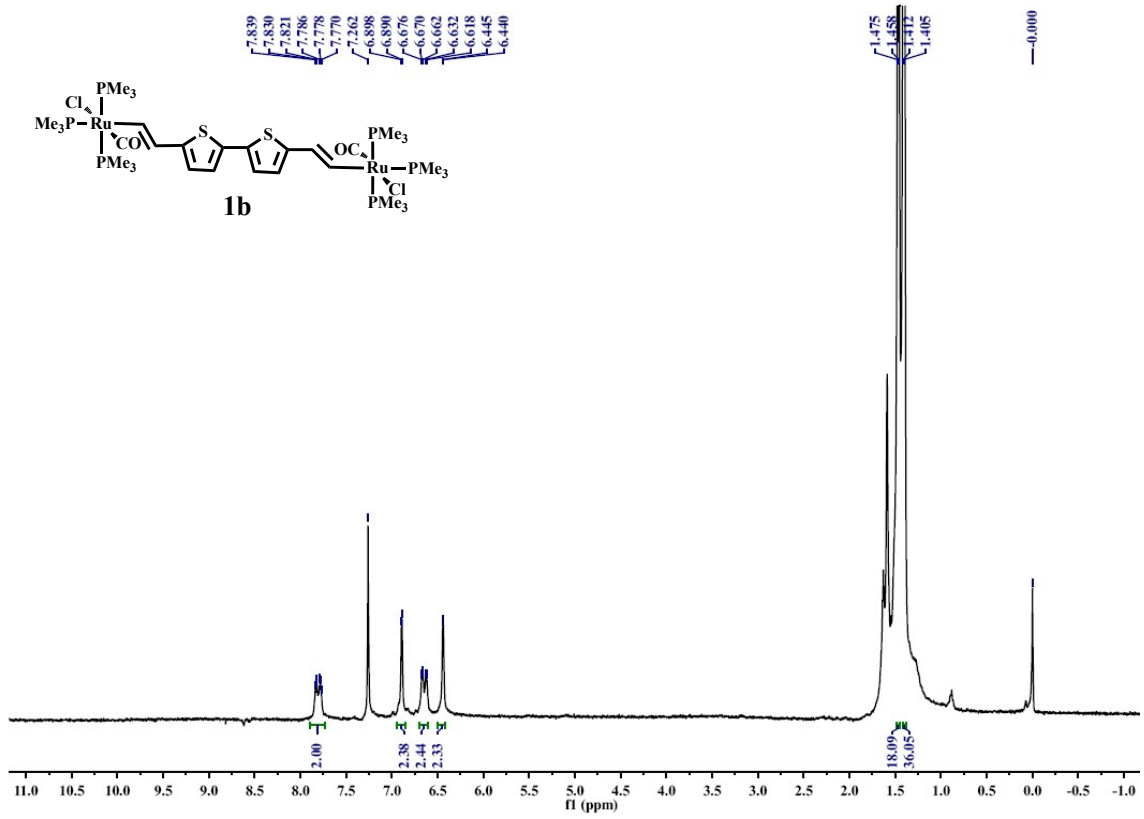

Figure S26. ^{1}H NMR spectrum (400 MHz, $CDCl_3$) of **1b**.

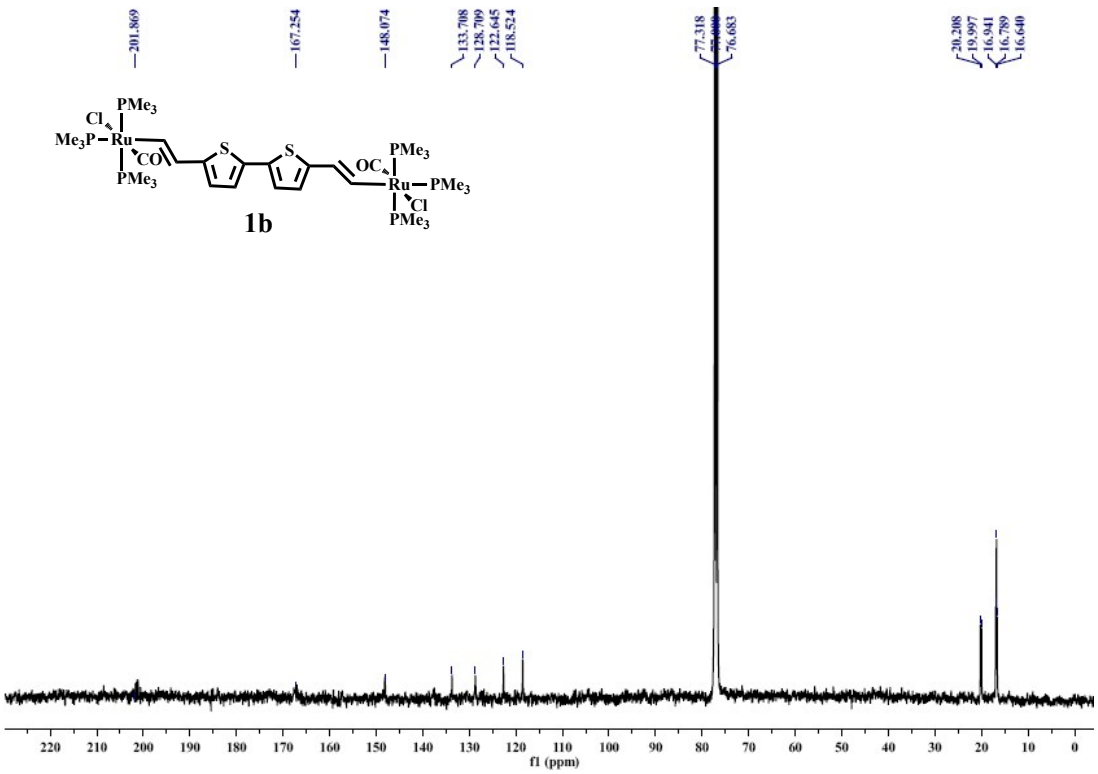

Figure S27. ^{13}C NMR spectrum (100 MHz, $CDCl_3$) of **1b**.

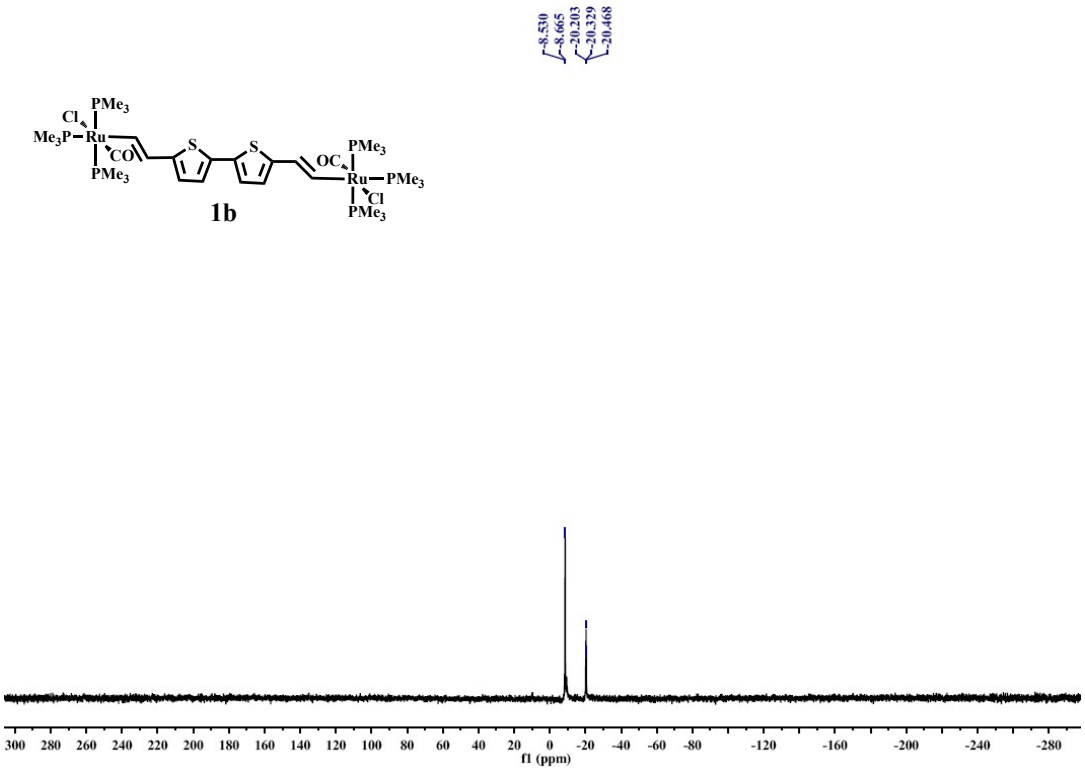

Figure S28. ^{31}P NMR spectrum (160 MHz, $CDCl_3$) of **1b**.

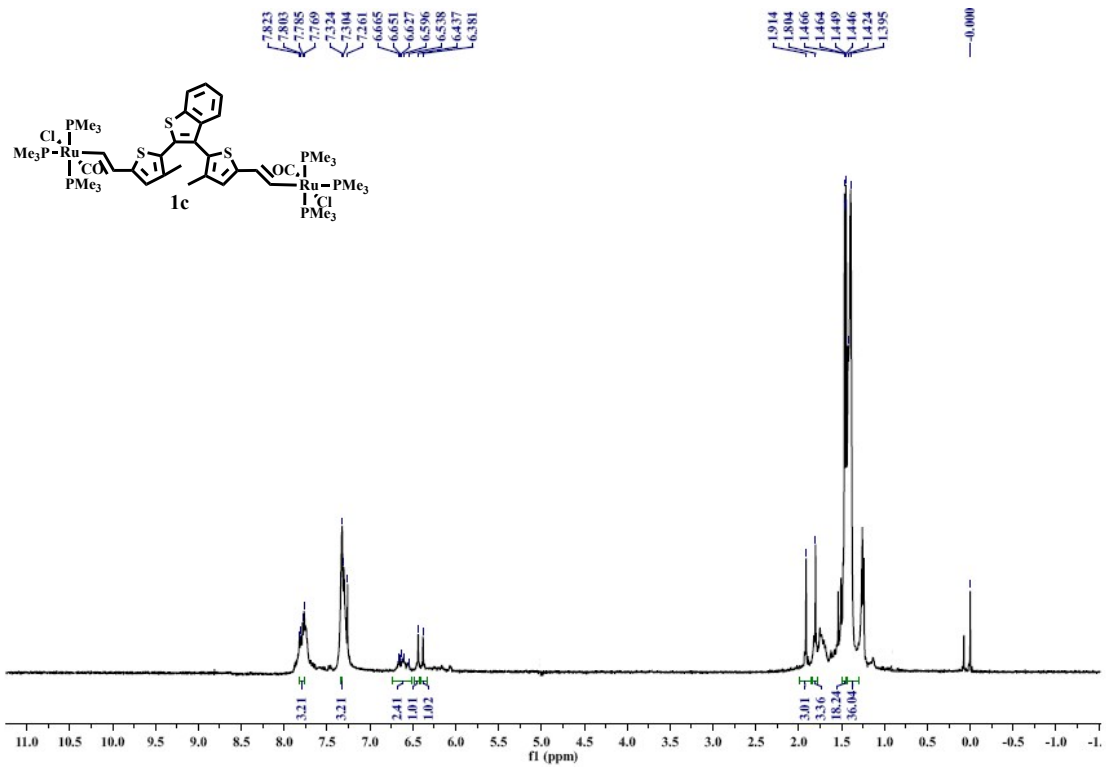

Figure S29. ^{1}H NMR spectrum (400 MHz, $CDCl_3$) of **1c**.

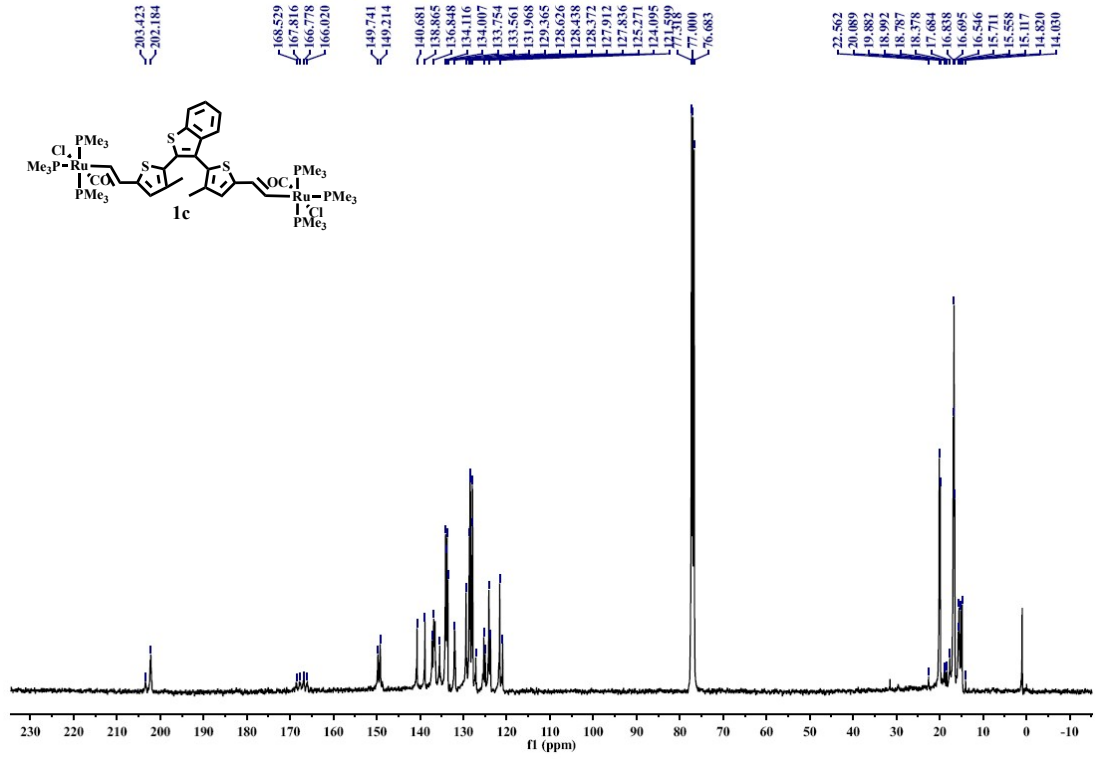

Figure S30. ^{13}C NMR spectrum (100 MHz, $CDCl_3$) of **1c**.

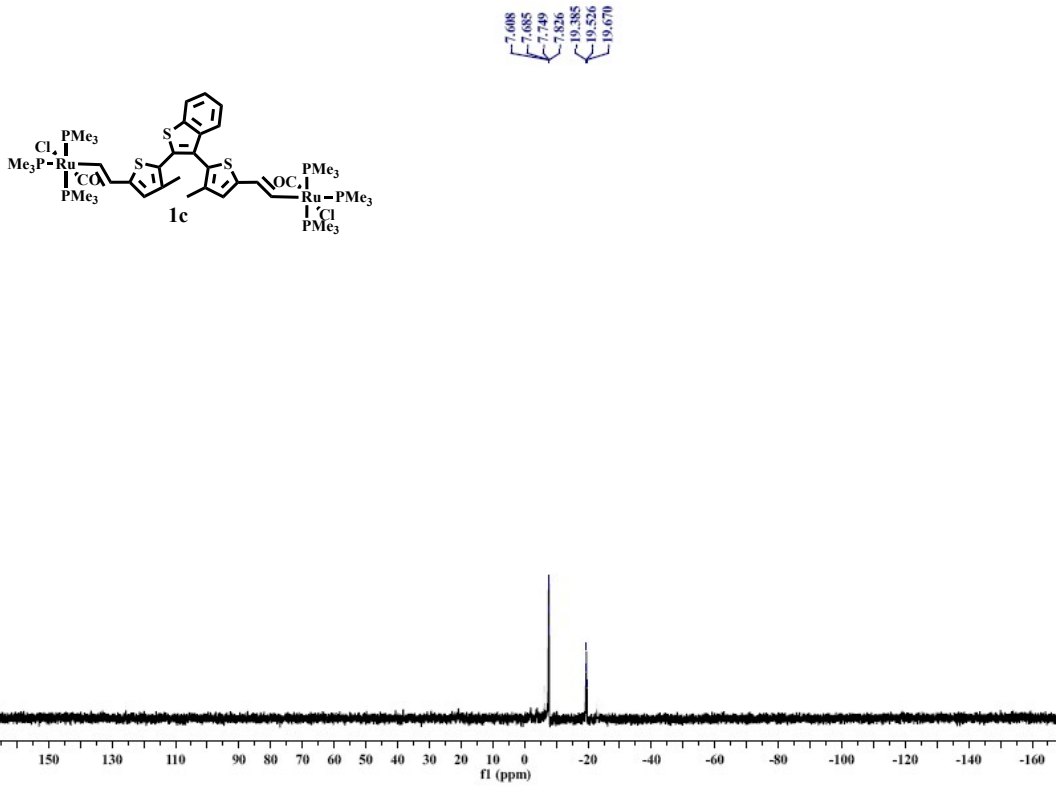

Figure S31. ^{31}P NMR spectrum (160 MHz, $CDCl_3$) of **1c**.

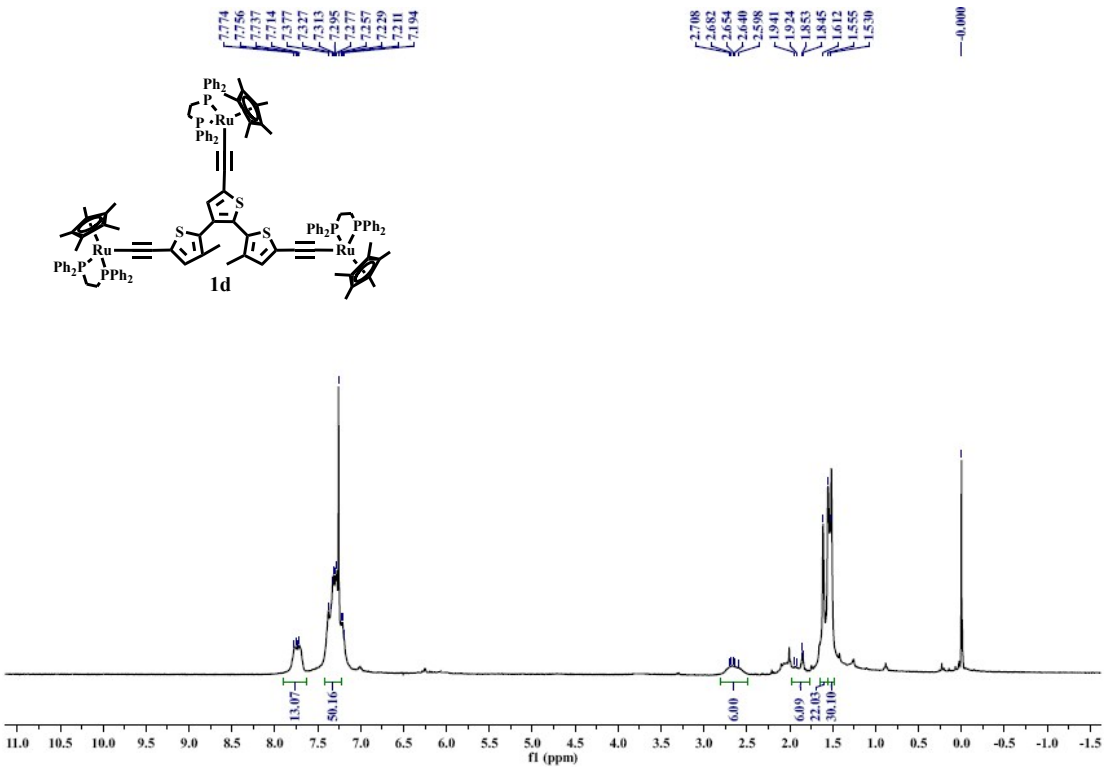

Figure S32. ^{1}H NMR spectrum (400 MHz, $CDCl_3$) of **1d**.

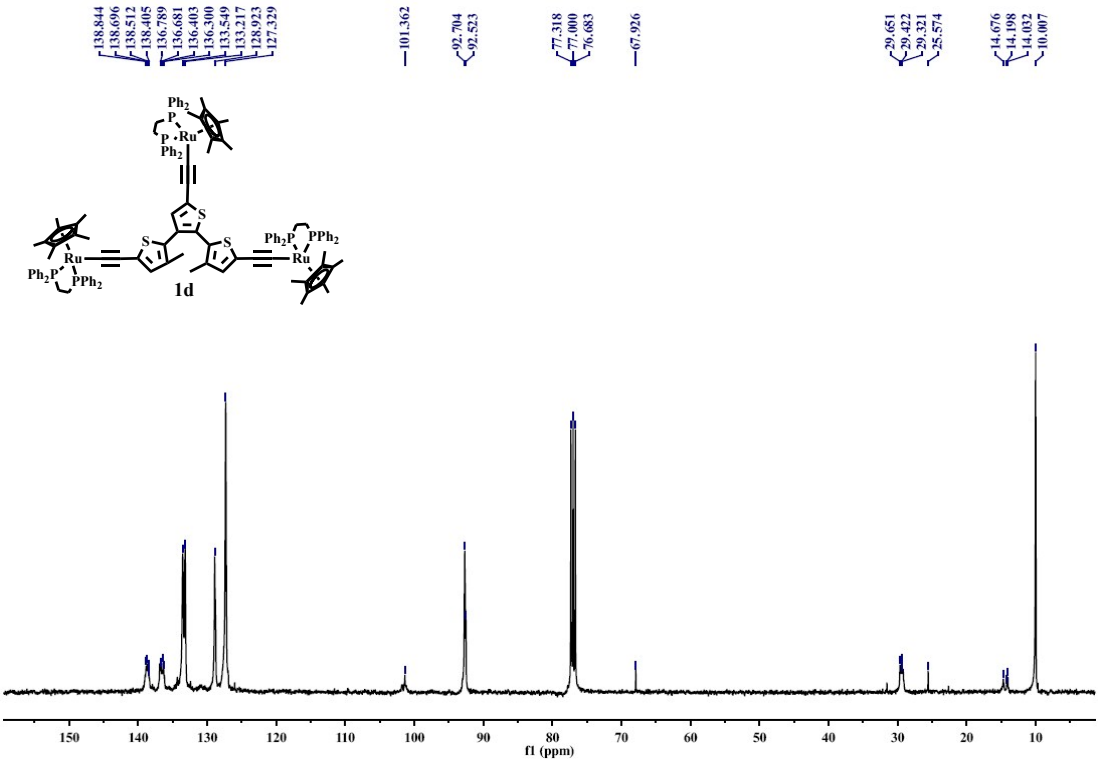

Figure S33. ^{13}C NMR spectrum (100 MHz, $CDCl_3$) of **1d**.

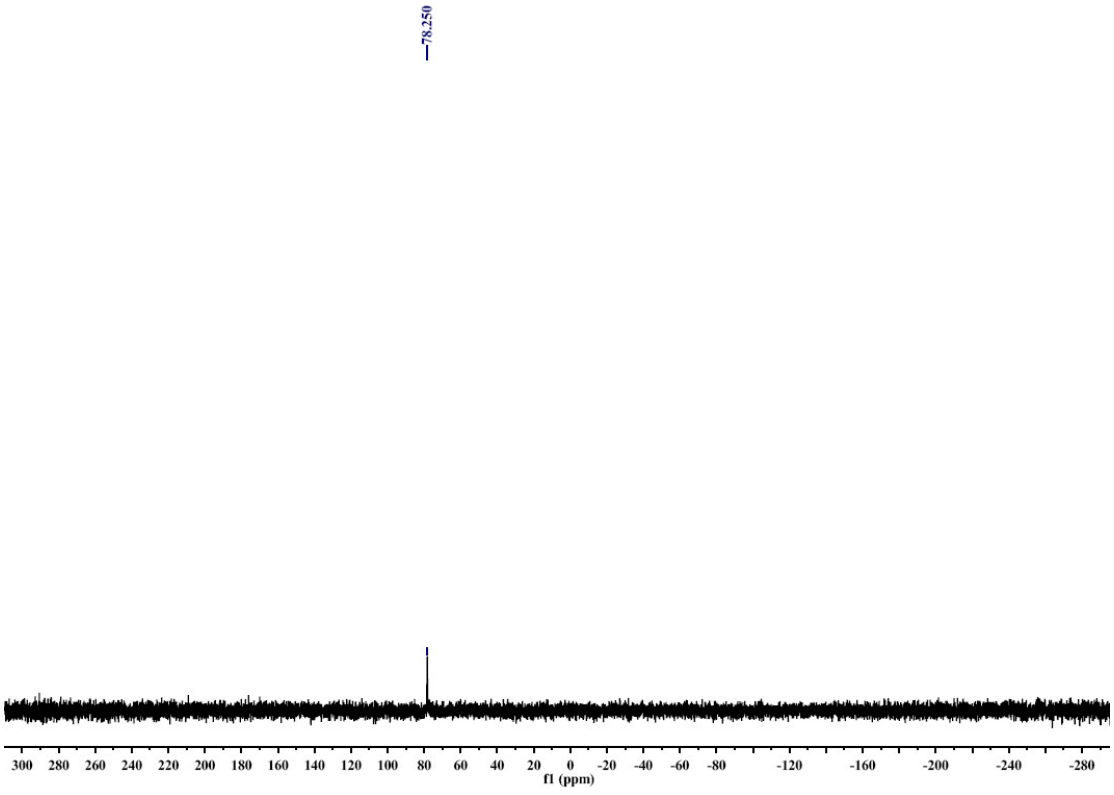

Figure S34. ^{31}P NMR spectrum (160 MHz, $CDCl_3$) of **1d**.